The Thesis Committee for Lucas Martin Holt

Certifies that this is the approved version of the following thesis:

Implantable Intracardiac

Bioimpedance System

APPROVED BY

SUPERVISING COMMITTEE

Supervisor: _____

Jonathan W. Valvano

_____

John Pearce

Implantable Intracardiac

Bioimpedance System

By

Lucas Holt, B.S.E.E

Thesis

Presented to the Faculty of the Graduate School of

The University of Texas at Austin

In Partial Fulfillment

Of the Requirements

For the Degree of

Master of Science in Engineering

The University of Texas at Austin

May 2014

Acknowledgements

My mom (The Mommy) has always had my back. In preschool, kindergarten, and grade school I was always the rowdiest in the bunch. I'm certain that many of my teachers tried to give up on me. I was labeled as ADHD, ADD, and dyslexic. Any and every reason to explain my craziness was used. The mommy had my back through it all. She made sure I wasn't getting left behind. She worked with the school to make sure I was being taught by the right teachers, set me up with special tutors, and put up with a whole lot of stuff that need not be mentioned in the context of a graduate thesis. In all honesty, I was no angel after grade school. I was still rowdy, but I wasn't labeled with learning disabilities and I always got straight A's. Thanks for putting up with all the problems I caused while growing up mom. I'm still a handful, but at least I know I've gotten to where I am today because you've always backed me up.

Over the years I've developed a strong work ethic when it comes to academics and industry. This is something that I know I've learned from the example of my father. Over the years, I have seen firsthand my dad's work ethic. This work ethic extends not only to his job, but also to his family. My brother and I both played travel ice-hockey while growing up. My dad always made sure that he could schedule his work around our practices and games. Not exactly sure how he kept up with both of us while pursuing projects at work with such intensity, but he more than made it work. Over the years, I've gotten to meet several of the people my dad works with. I can always see the respect they have for him. This respect is a result of both my father's work ethic, and the sincere way that he treats the people around him. Someday I hope to achieve the same level of respect that my father has earned from his peers.

I consider myself one of the lucky ones. This thesis and my overall graduate experience involve working and learning about things that truly interest me. Over the course of my academic tenure at the University of Texas at Austin I have developed a strong working relationship with my mentor Dr. Jonathan Valvano. He and I seem to think about problems in a similar way most of the time. Even more importantly, he and I seem to think about problems differently some of the time. These are important factors that drive collaboration and creativity between two people. Throughout my graduate research, he has always encouraged me to focus on the right problems at the right time. Additionally, he provides a level of enthusiasm to ideas that cannot be mimicked. No matter how big or small the idea may be Dr. Valvano seems to find a spark of passion within himself that he very easily passes on to those around him.

From before I even started graduate school, the words of Dr. John Pearce have stayed with me. On the way out of his office one day, he said something to the effect of, "Lucas, we'll make an analog guy out of you yet". In taking Dr. Pearce's courses, I developed a set of fundamental analog skills that have enabled me to solve problems that I would have previously been oblivious too. I truly think that this skill set is something that will set me apart from other engineers throughout my career. Dr. Pearce, hasn't made me an "Analog Guy" but he has begun to make me a "Mixed Signal Guy".

From the first year of my undergraduate degree at UT, Dr. Earl Swartzlander has been my friend and mentor. He was the first person who got me thinking about the idea of graduate school. Additionally, he was the first professor who encouraged me to work on projects outside of the class room that were interesting to me. He answered my questions, got excited about my results,

and encouraged me to keep exploring. Over the past 5 years, I have gone to Dr. Swartzlander for advice, good conversations, and friendship. There are a handful of people in my life who I have relied on when making important decisions during college. Dr. Swartzlander is one of them.

Dr. Marc Feldman – For answering all my basic cardiology questions and setting my dad straight on coconut oil.

Kelvin Le - For Putting up with my shenanigans in the lab, and helping me work through circuit analysis problems that were over my head.

Andrew Wang – For playing good music, keeping things easy going in the lab, and being tremendously buff.

Ben Bright - For hanging out with me in the lab pounding green tea until 2:00am.

Dr. Anil Kottam - For showing me how methodical thinking can be applied to even the simplest task, like mixing saline solutions efficiently.

Dr. John Porterfield – For organizing our large scale experiments, which allowed me experience some things that I will never forget.

Abstract

Implantable Intracardiac

Bioimpedance System

Lucas Martin Holt, M.S.E

The University of Texas at Austin, 2014

Supervisor: Jonathan W. Valvano

An implantable intracardiac bioimpedance system has been designed to measure the real and imaginary parts of impedance in a dynamic cardiac setting. The system is broken into two parts: an implantable wireless device and a desktop base station. This measurement is performed using both tetrapolar and tripolar electrode configurations where a 20 kHz current field is applied to the intracardiac blood pool and myocardium. Epochs of discrete voltage samples from the resulting electric field are analyzed using a digital signal processing algorithm to generate impedance measurements. Measurements are then wirelessly transmitted from the implantable device to a base station where advanced signal processing algorithms are applied and the data is plotted in real-time. The final system measures 485 impedance samples/sec, consumes 50 mA when active, and has a percent of measurement error less than 1% for the intracardiac bioimpedance range. The device has been extensively tested to ensure the quality of measurements required for future human use. Instrument design, calibration, verification, experimentation, and modeling are the primary topics of this thesis. Moving forward, the system will be used in studies where dynamic bioimpedance signals measured in the right and left ventricles of the heart will be used to derive stroke volume.

Table of Contents

List of Tables

List of Figures

Chapter 1: Introduction

1.1 Motivation

Electro-physiologists lack the ability to continually monitor stroke volume in patients who have been implanted with cardiac resynchronization therapy (CRT) devices. A relative stroke volume measurement that requires minimal hardware change in existing CRT technology will give CRT companies a powerful decision-making tool. The metric can be used as an input to algorithms that CRT devices use to make decisions on how to control a patient's heart. Additionally, changes in heart volume can be used to detect early signs of heart failure [7]. Intracardiac bioimpedance derived volume is a solution to these problems that requires no mechanical and minimal electrical design changes in existing CRT technology.

CRT devices are broken into two categories: pacemakers (CRT-P) and defibrillators (CRT-D). Pacemakers are designed to measure activity in the heart and correct improper activity by depolarizing the myocardium cells with stimulation current. Defibrillators have the added feature of a reset button for the heart. A patient experiencing a cardiac arrhythmia, such as ventricular tachycardia (vtach) or ventricular fibrillation (vfib), will be automatically defibrillated by their CRT-D in an attempt to reset the heart to normal rhythm. This reset is performed through the same mechanism that CRT-P devices employ. However, the required stimulus is orders of magnitude larger in CRT-D devices. The myocardium of the heart is depolarized using an electrical stimulus. In the case of a defibrillator it is not a local depolarization. The myocardium most of the heart is depolarized with a single burst of electrical energy. All of the myocardium cells undergo a simultaneous refractory period, and then return to normal cardiac operation [9].

Currently, shocking algorithms in CRT-D devices are decided upon by intracardiac ECG signals measured by the CRT device. As a result, up to 1/5 of all patients with CRT-D devices experience shocks that are inappropriate [6]. A bioimpedance-derived stroke volume measurement will add reliability to these imperfect shocking algorithms.

CRT devices are optimized for their patients only at the time of implant; over time, as a patient's physiology changes, efficiency can be lost. Using stroke volume as an input, pacing algorithms can tune a patient's cardiovascular operation for optimized efficiency. This can improve patient longevity and quality of life in the long term.

Research has shown that right ventricular (RV) hemodynamics are a strong indicator of heart failure [7]. Continued diagnosis of stroke volume in a patient will provide doctors with a powerful decision-making platform. Using this information, a physician can make informed decisions about a patient's health, deciding on ways to further diagnose the problem.

The stroke volume measurement must not affect the basic operation and structure of the current CRT devices. CRTs are composed of electrical components for measurement and control, a case for support and sterility, and electrodes for interface with a patient's heart. By making minor changes to the electrical components inside the CRT, an intracardiac bioimpedance signal can be leveraged using the existing electrode technology.

In the long-term, a device that accurately measures intracardiac bioimpedance-derived stroke volume will serve as an important tool for doctors and CRT device companies. Including this lightweight technology, existing CRT device architectures will save and improve the lives of the approximately 600 thousand patients who are implanted with CRT devices yearly [8]. To prove that this technology is viable, a precision implantable intracardiac bioimpedance system

was developed, tested, and validated. Moving forward, the system will be the cornerstone of large animal and human studies to validate the measurement.

1.2 Previous Research and Devices

Previous bioimpedance systems for intracardiac measurements have either been high-resolution non-implantable or low power implantable. In general, high-resolution non-implantable systems are primarily analog, using a synchronous demodulation implementation [2]. In the past, these systems have been used to measure intracardiac bioimpedance signals in both large animals and rodents. Commercial implementations of the analog system have been developed by Transonic Scisense Inc. under their Advantage Pressure Volume product line. This system has been used in cardiovascular hemodynamic research around the world [5]. However, power and size limitations of these analog systems limit their use as implantable devices. Implantable systems for measurements in rodents have been developed using a mixed-signal architecture [1]. In them, bioimpedance measurements are derived from a short-time signal processing algorithm. Typically these systems have suffered from tradeoffs between accuracy and necessary specifications for implantation.

1.3 Design Goals

The implantable intracardiac bioimpedance device is designed to be small, low-power, and wirelessly capable with minimal impact on performance. Design objectives are listed in Table 1. The size should be less than 3in x 2in x 1in to minimize discomfort for large animals that have been implanted. The device should be able to transmit at least 20ft through 2in of tissue. To ensure the accuracy of derived stroke volume calculations, measurements should have a percent of measurement error less than 1% for the intraventricular bioimpedance range. To ensure adequate resolution, a signal to noise ratio (SNR) greater than 1000 at half of full scale

should be achieved. To precisely analyze a dynamic intracardiac bioimpedance signal, at least 100 samples per heart cycle should be taken. Since a large animal has a maximum heart rate of 220 bpm, or 3.66 Hz, the device should have a sampling rate of at least 366 Hz. The device should be able to continuously capture data and wirelessly transmit the samples to the base station for 15 hours. Size limitations of the device restrict the lithium ion battery size to 1000 mAh. Given these requirements, the device must consume less than 67 mA of current in continuous measurement mode.

Table 1: Desired Device Specifications

Desired Device Specification	**Value**	**Special Note**
Dimensions	<2inx3inx1in	
Transmission Distance	>20 ft	through 2in of tissue
Percent of Measurement Error	<1 %	
Signal to Noise Ratio	>300	
Measurement Frequency	>367 HZ	
Battery Life Continuous Mode	>15 hours	with 1000mAh battery

These aggressive design goals were derived from the system specifications of previous analog and mixed signal implementations. Compared to the previous mixed signal system, size and power consumption have both increased by a factor of 2 [1]. However, the measurement specifications have remained on par with previous analog implementations of the device [2]. The primary goal of this device is to create a bioimpedance implant that does not sacrifice precision when compared to its analog predecessors.

1.4 Terminology and Background

Before discussing the specific application of a bioimpedance measurement, a brief overview of impedance and its derivatives are necessary. To start, an explanation of what physically creates the values of an impedance measurement is given. Additionally, different

forms of load analysis, such as admittance, are introduced. Lastly, a discussion of phase and magnitude are provided.

1.4.1 Physical Sources of Impedance

Impedance is a load measurement that describes how resistive a circuit is to a change in current. The impedance of a circuit is determined by the value and orientation of the basic elements that comprise it. The real part of impedance is resistance. The imaginary part of impedance is reactance. In general, these fundamental equations define impedance, Z, and the impedance contributed by resistors, capacitors, and inductors. R is resistance in ohms (Ω), X is reactance in (Ω), C is capacitance in farads (F), L is inductance in henrys (H), w is frequency in (rad/s), and j denotes an imaginary unit.

$$Z = R + jX$$
$$Z_R = R$$
$$Z_C = \frac{1}{jwC}$$
$$Z_L = jwL$$

1.4.2 Admittance and Impedance

Admittance is another load measurement defined as the inverse of impedance; it is sometimes a much simpler way to analyze the properties of a circuit. Since it is described as the inverse of impedance, admittance is a measure of how easily a circuit allows current to flow. Although the instrument discussed in this thesis measures impedance, its measurements can be used to obtain admittance. Some forms of derived stroke volume are much simpler to analyze in terms of admittance. In short, admittance is an effective way to analyze circuit models where all components are in parallel; impedance is more useful for analyzing circuits where all components are in series. Biological systems invariably consist of a mixture of parallel and series components. The following equations define admittance, Y, in terms of impedance. Like

impedance, admittance is a complex number. The real part of admittance is conductance. The imaginary part admittance is susceptance. In the following equation, conductance is G and susceptance is B; both in siemens (S).

$$Y = G + jB$$

$$Y = Z^{-1} = \frac{1}{R + jX} = \frac{R - jX}{R^2 + X^2}$$

$$G = \frac{R}{R^2 + X^2}$$

$$B = \frac{-X}{R^2 + X^2}$$

1.4.3 Phase and Magnitude

Impedance and admittance can be analyzed in terms of either real and imaginary or magnitude and phase. Sometimes, it is useful to interpret admittance and impedance signals in terms of magnitude and phase. Phase has the unit of radians (rad) for both admittance and impedance. In most cases, the phase is multiplied by 180/π to convert it to degrees (°). The magnitude of admittance has the unit (S). The magnitude of impedance has the unit (Ω).

$$|Z| = \sqrt{R^2 + X^2}$$

$$\angle Z = \text{atan}\left(\frac{X}{R}\right) \; if \; R > 0$$

$$|Y| = \sqrt{G^2 + B^2}$$

$$\angle Y = \text{atan}\left(\frac{B}{G}\right) \; if \; G > 0$$

1.5 Circuit Models For Intracardiac Bioimpedance

Simplified circuit models for the interaction of muscle (myocardium) and blood are the basis for intracardiac bioimpedance measurements. In general, two basic circuit models are accepted: a cross ventricular series model [3], and an intraventricular parallel model [10]. In humans, a cross ventricular series model is useful for deriving left ventricular stroke volume

measurements. Whereas, an intraventricular parallel model is better suited for calculating right ventricular stroke volume.

The myocardium of the heart is approximated to be a parallel combination of resistance and capacitance. The capacitive component of the myocardium is the result of living myocyte membrane. Since the cell membrane is selectively permeable to certain ions, it acts as a charge separator. This is comparable to the properties of the dielectric for a capacitor. The resistive component of the myocardium comes from the extracellular fluid surrounding the myocardium as well as the resistive properties of the cell membrane.

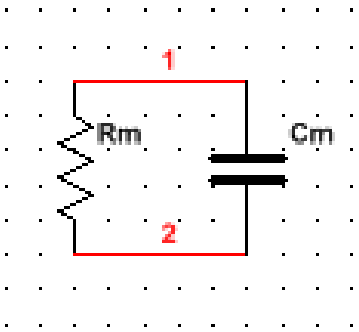

Figure 1. Myocardium Circuit Model

In a, cross ventricular measurement, the resistance of the ventricular blood pool is mostly in series with the myocardium. The measurement is made from the outside of the free wall in the left ventricle to the septal wall of the right ventricle. Since the measurement is made from the exterior of the left ventricle, the current field passes through the myocardium first and then passes though the left ventricular blood pool. For this reason, the approximated circuit model has the blood resistance in series with the myocardium circuit model. This model has both series and parallel components. It is therefore more difficult to analyze, and there is no apparent benefit to using admittance or impedance.

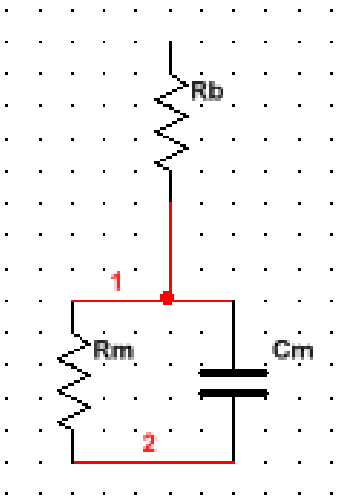

Figure 2. Cross Ventricular Circuit Model

For the intraventricular parallel model, the resistance of the ventricular blood pool is primarily in parallel with the myocardium. For this measurement, a single shaft with multiple electrodes is placed into the right ventricle of the heart. The current field emanates from the center of the blood pool passing through both myocardium and the blood pool at the same time. Since the current field passes through both components of the model at the same time, a parallel circuit model is appropriate. Since all components are in parallel, it is beneficial to analyze the circuit in terms of admittance.

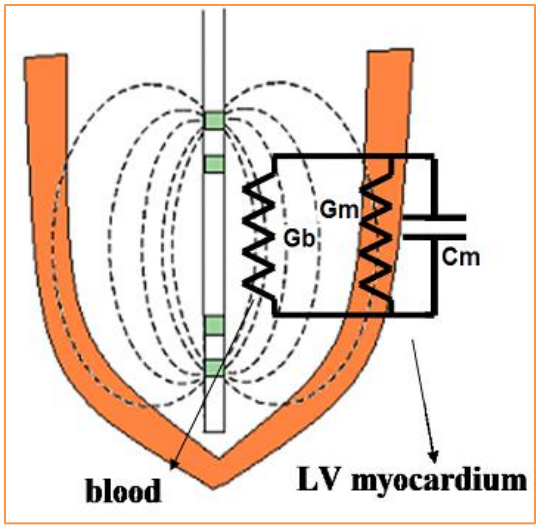

Figure 3. Intraventricular Circuit Model

1.6 Measurement Method

In theory, measuring impedance is a simple application of Ohm's law. The process begins with an ideal alternating current (AC) source of known phase and magnitude. The current source is applied to the load of interest. Then, the resulting voltage across the load is measured. To calculate the impedance of the load, the output voltage is divided by the input current. Using phase and magnitude, or phasor notation, this calculation becomes trivial. The following equations describe this process using phasors and ohm's law.

$$|V|\angle V = |I|\angle I \times |Z|\angle Z$$

$$\frac{|V|\angle V}{|I|\angle I} = |Z|\angle Z$$

$$|Z| = \frac{|V|}{|I|}$$

$$\angle Z = \angle V - \angle I$$

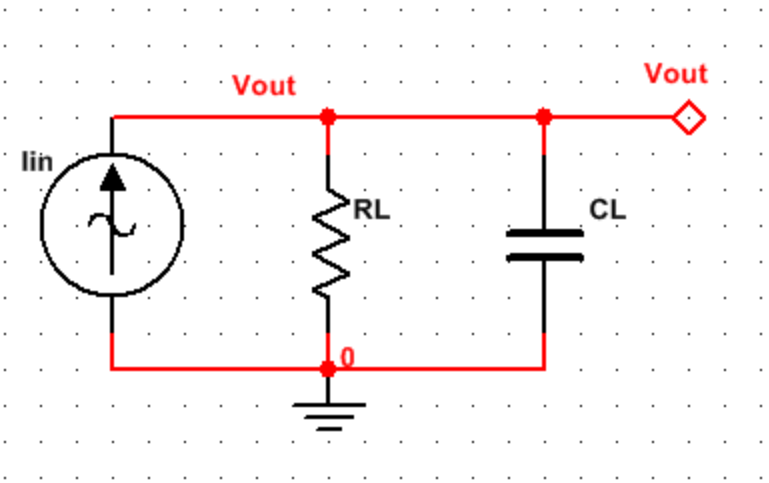

Figure 4. Theoretical Impedance Measurement

This fundamental equation applies for bioimpedance as well. In a traditional circuit, charge is carried by the free electrons on the surface of a metal. By contrast, in a biological system charge is carried by ions such as sodium (Na+) and chloride (Cl-). In a biological system it is easier to think of voltage in its traditional form, an electric field. Therefore, ohm's law is applicable:

$$\vec{J} = \sigma\vec{E}$$

Where, J is current density (A/m^2). E is, electric field (V/m), and σ is conductivity (S/m)

Chapter 2: Implementation

2.1 Top Level System

The system is made up of two primary components, the implantable device and the base station. The implantable device acquires the raw impedance signal and wirelessly transmits it to the base station for processing. The base station consists of both an access point and a front end application. The access point acquires the data from the device, and the front end application handles display, interpretation, and storage of the data.

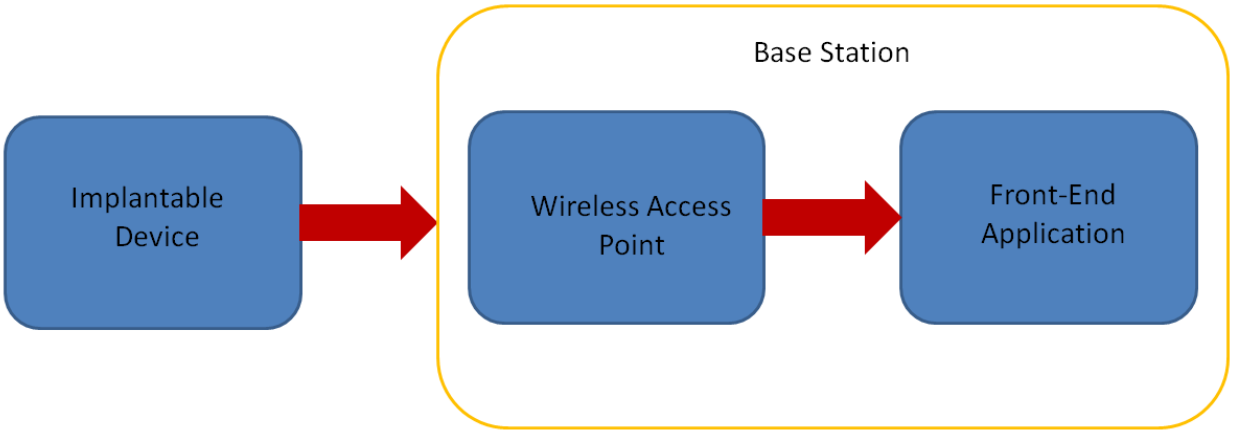

Figure 5. System Block Diagram

2.2 Implantable Device

The implant was designed to be accurate, low-power, and wireless -apable. To ensure quality of measurement, high performance active components were selected. To ensure low-power operation, a mixed signal implementation was chosen. The CC430F5137 microcontroller from the MSP430 processor line was selected because of its low power MSP430 characteristics and its wireless communication capabilities.

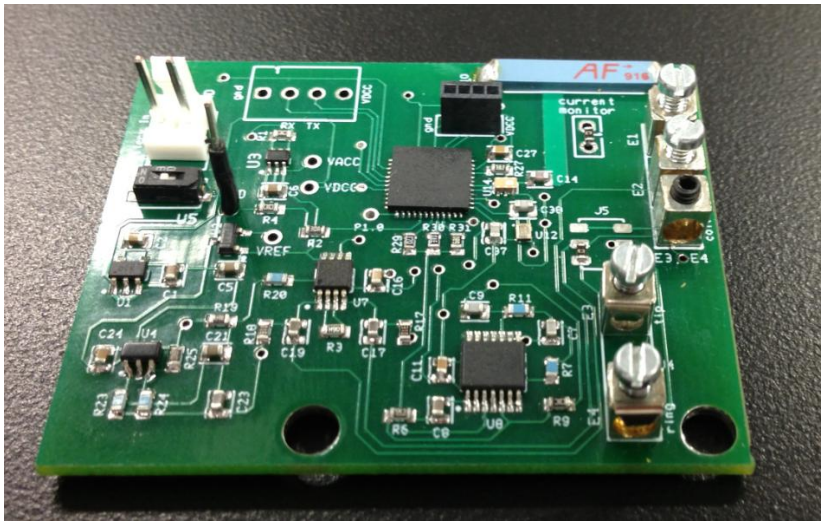

Figure 6. Implantable Device

Table 2: Achieved Device Specifications

Achieved Specification	**Value**	**Special Note**
Dimensions	<2inx3inx1in	
Transmission Distance	>50 ft	through 2in of tissue
Percent of Measurement Error	<1 %	
Resolution	.05 ohms	
Measurement Frequency	488 HZ	
Battery Life Continuous Mode	20 hours	with 1000mAh battery

2.2.1 Mixed Signal Processing

A mixed signal architecture was used because of the size and power constraints associated with the implantable device**.** The measurement begins with the generation of a phase reference current source. This current source is applied to the biological tissue of the heart and the resulting electric field is measured**.** The analog electric field measurements are conditioned by analog filters before they are sampled by the analog to digital converter (ADC) of the microcontroller. Once the electric field has been digitized, epochs of data are run through an

assembly optimized signal processing. The outputs from the digital algorithm represent the measured bioimpedance at a specific instance in time.

2.2.1.1 Current Source Generation

A reference phase current source is generated by the microcontroller using a basic digital to analog converter (DAC), several signal conditioning op-amps, and an op-amp in a current source configuration. It is designed to have an RMS current of 100 uA and at a frequency of 20 kHz. The digital outputs of the microcontroller are generated in a way that allows the current source to behave as a phase reference for the voltage signal.

The DAC is connected to an output port. Since the DAC has a finite number of discrete voltages, a 2-pole Sallen Key low pass filter is used to smooth the DAC output. Once conditioned, the voltage signal from the DAC is fed to a voltage to current convertor. The output current across the load is a linear function of the input voltage.

$$I = \frac{Vin}{RS}$$

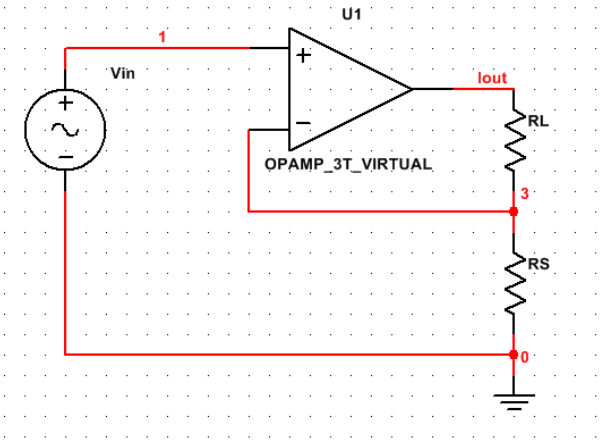

Figure 7. Op-amp Current Configuration

The high-level process is as follows: the DAC is used to create the current and the ADC is used to measure the resulting voltage. Signal processing allows for impedance to be measured from the ADC samples.

2.2.1.2 Electric Field Measurement and Conditioning

The electric field is measured using an instrumentation amplifier that has its positive and negative terminals across a section of the heart using intracardiac CRT electrodes. Since the current source is not to exceed 100 uA RMS, the resulting electric field within the cardiac system is small. The typical sensing region within the heart has an equivalent load of less than 100 Ω. The gain of the instrumentation amplifier is set to achieve maximum peak to peak output swing for a 100 Ω load assuming a 100 uA RMS current source. Doing this ensures the maximum common mode rejection ratio for the instrumentation amp.

To remove non-linearity associated with the electrode electrolyte interface, the electric field measurement is ideally performed in a tetra-polar configuration. The current source and voltage sensing nodes are separated from each other. In the following picture: nodes 1 and 4 represent current source electrodes and nodes 2 and 3 represent voltage sensing electrodes. Hence, to make a bioimpedance measurement four electrodes should be used. A more detailed explanation on this topic will be provided in Chapter 5.

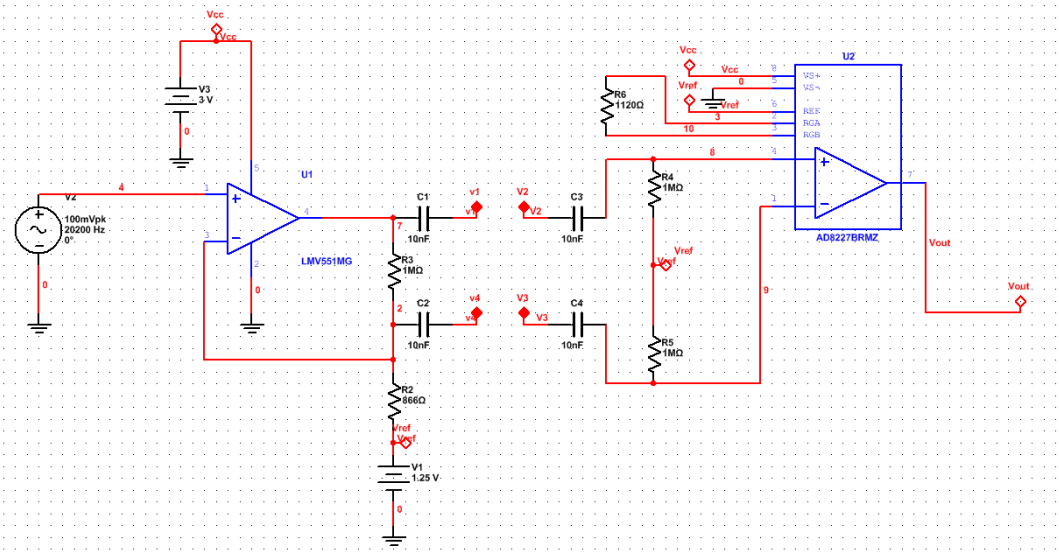

Figure 8. Electric Field Measurement

After the instrumentation amplifier, the electric field signal is put through a band-pass filter. This filter's primary purpose is to act as an anti-aliasing filter for the digital domain. However, it was chosen to be a band pass filter in order to attenuate low-frequency differential signals present in the body.

2.2.1.3 Short-Time Signal Processing Function

Epochs of discrete electric field samples are analyzed using a single bin short-time signal processing algorithm. This algorithm allows the determination of the complex electrical properties in real time. An epoch of data is fed into the algorithm at a fixed sampling rate. The output of the algorithm is proportional to the bioimpedance of interest (See Appendix). Given these specifications, an assembly optimized signal processing algorithm was developed using less than 150 add and shift operations. This allows the device to capture impedance samples at a rate of 485 Hz. Since the cardiac system is dynamic, a sampling rate much greater than the heart rate frequency is necessary. Assuming a maximum heart rate of 220 bpm or 3.66 Hz the implantable device is capable of capturing over 130 bioimpedance samples per heart beat.

2.2.2 Power Management

The implantable device supports two forms of low power operation: MSP430 low power mode 3 (LPM3) with analog power disable, and magnetically controlled reed switching. In both cases, the purpose is to put the device in sleep mode when impedance measurements are not being made. This is important energy saving feature for implantation. While impedance measurements are being made 50mA of current is consumed. With a 1000mAhr battery, 20 hours of impedance data can be collected. By placing the device into sleep mode, the 20 hours of data collection can be dispersed across the required length of time the implant must run.

To achieve low power operation using software a combination of built in processor capabilities and analog power disabling is used. LPM3 is a built in sleep state of the CC430F5137 and other MSP430 microcontrollers. By issuing a software command, the user can put the processor into LPM3. However, the analog components present on the device will still be active. To solve this issue, paired p-channel n-channel MOSFETS are used. A GPIO pin controls the gate of the n-channel MOSFET which controls the supply voltage to the analog section of the chip using a p-channel MOSFET. To properly put the implant into LPM3, the user must perform the following actions: disable analog power using the GPIO pin, turn off OSC2 (RFCLK), set the MCLK, SMCLK, and ACLK source the VLO (Very Low Power) 10 kHz oscillator, initialize a timer interrupt to wake the device from LPM3, make all port pins grounded outputs, and finally set the appropriate system register bits to instantiate LPM3. In theory, the processor consumes 7uA of current in LPM3. The implantable intracardiac system consumes 45uA in LPM3. This is most likely the result of current leakage to ground in the regulator.

A magnetically controlled reed switch is an alternative form of low-power control. This much simpler solution, places a magnetically controlled reed switch at the power trace coming

from the battery. When a magnet is placed over the device, the switch is closed and the implant runs in continuous mode. When the magnet isn't present, the switch is open and the implant is completely off. This solution significantly decreases the complexity of the software and drops current consumption to 0uA when off. However, there is the added difficulty of having to strap a magnet to the subject when measurements are being taken.

2.2.3 Communication

A wireless communication channel is used to send impedance samples from the implantable device to the desktop base station for processing. The CC430F5137 microcontroller comes with a built-in RF block. The RF block internal to the CC430F5137 MCU is a CC1101 RF core. For optimized data transmission a predefined stack protocol is not used. The CC1101 RF core is configured with a custom initialization routine, and an application specific communication packet for impedance measurements has been developed. The hardware capabilities for error detection in the CC1101 RF core are enabled. Error correction methods were not utilized; in the event of error detection the packet is discarded. To change the initialization routine TI Smart RF Studio should be used. Using this Texas Instruments (TI) application support software for the RF core settings can be easily changed. The tool gives users the ability to change characteristics such as: base frequency, modulation format, channel number, data rate, channel spacing, and transmit power.

2.3 Base Station

The purpose of the base station is to receive, process, plot, and save wireless impedance measurements from the implant in real-time. It consists of two parts: a wireless access point and a desktop computer with front end application software. The wireless access point uses a CC4306F137 to communicate with the CC430F5137 in the implant. It sends the received

wireless packets to the desktop computer using a USB interface. The front end application software is written in a scripting language called Processing. This java derived language was selected because of its built in rolling graph library.

2.3.1 Access Point

The access point, designed by Katy Loeffler [1], communicates wirelessly with the implant using an EM430F6137RF900 evaluation module, and then passes the wireless communication packets via USB to the desktop computer. The EM430F6137RF900 evaluation module produced by Texas Instruments has a CC430F6137 microcontroller on it. Both the CC430F6137 (access point) and the CC430F5137 (implant) have CC1101 RF cores. This means that they are able to communicate wirelessly with one another. The PCB developed by Katy Loeffler [1] has burg headers to interface with the EM430F6137RF900 evaluation module, 4 LED indicators, and a UART to USB chip. The evaluation module receives the RF packets and sends them to the computer though UART. The UART to USB conversion chip then sends the packets in USB format to the desktop computer. The communication packets from the access point are received by the desktop computer using a standard COM port interface. At this point the front end application takes over.

2.3.2 Front End Application

The front end application unpacks, processes, plots, and saves the data from the COM port using a scripting language called Processing. The USB data packets are packed using an algorithm that Dr. Valvano developed. The packing algorithm is similar to a standard binary coded decimal format. In short, the algorithm assures that no zeros are transmitted in the data. This is done because zeros are used to indicate the end of a packet. The first job of the front end application is to reverse the packing algorithm, converting the USB packet back to its original 16

bit signed integer format. The raw real and imaginary impedance values are stored to an archive file before any processing is applied. Archiving the raw data allows for alternative analysis techniques to be used in post processing. The real and imaginary impedance values are then processed. Firstly, they are both run through an FIR filter with 15 Hz cutoff and 25 Hz stop band. The maximum heart rate for a large animal is around 3 Hz (180BPM). Hence, a 15 Hz cutoff allows for analysis of at most the 5^{th} harmonic of heart rate in large animals. Next, the real and imaginary components of the impedance measurement are used to isolate the resistive contribution from the blood. One of two equations to isolate the resistance contribution from the blood must be selected. The first assumes that the blood and muscle in the cardiovascular impedance measurement are in parallel with each other [5]. The second assumes that the blood and muscle of the cardiovascular impedance measurement are in series with each other [3]. Reasons for the selection of each model will be discussed in depth in chapter 5, but for now it is important to know that the front end application allows the user to select between the two analysis techniques in real-time. By analyzing isolated resistance samples from the blood as a function of time, a relative stroke volume measurement is derived. The simplest analysis technique is to take the maximum minus the minimum of the isolated resistance of the blood over a given cardiac cycle. The front end application saves and plots each of these four channels: filtered real, filtered imaginary, isolated blood resistance, and derived stroke volume. The real-time plot allows for easy visualization of data during experiments, and the saved tab delimited files allow for analysis after the experiment.

Chapter 3: Evolution and Manufacturing

3.1 Evolution of Device

The device has evolved through 5 PCB revisions for reasons such as: performance, hardware bugs, and form factor. Revision one was intended to explore a variety of circuit implementations. Using the first revision, the optimal circuit implementation was realized. In revision two, most of the optional circuit configurations were removed. Only one configuration option was left on the board. Revision three removed the final optional circuit configuration. It also fixed a bug that caused the wireless communication not to function. Revision four altered the form factor of the device. In previous revisions, the device was connected to pacing leads using alligator clips. In revision five, the alligator clips were replaced with screw tap terminals. Revision five increased mechanical reliability and wireless transmission range.

3.1.1 Revision 1

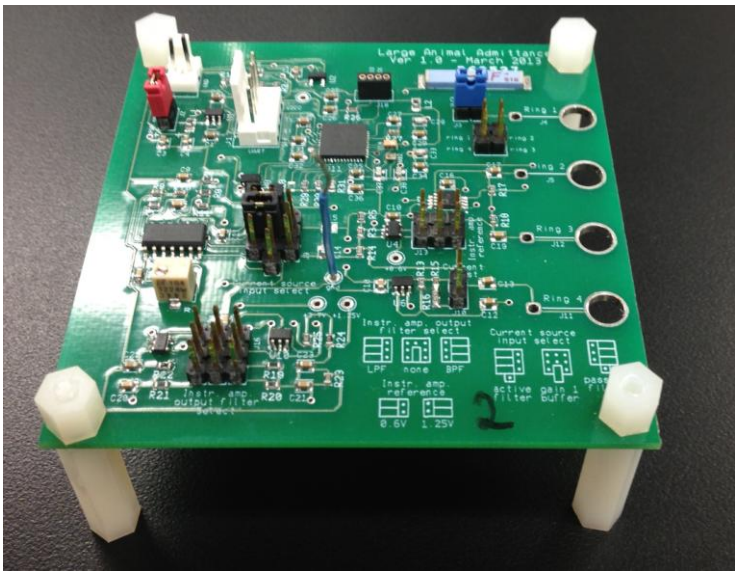

Figure 9. PCB Revision One

The first revision of the device was used for circuit exploration. In the bottom right-hand corner a jumper key is provided. This key allows the user to select among the different circuit

configurations that are available. Circuit options revolve around 3 features: output filter, current source input, and instrumentation amplifier reference voltage. Additionally, a single turn pot allows for the adjustment of the stimulation current. The output filter has three possible options: low pass filter, band-pass filter, and none. The current source can be driven with an active, passive, or gain one signal source. The instrumentation amplifier reference can be set to either 1.25 V or 0.625 V. All possible configurations were tested for accuracy (expected value) and resolution (standard deviation). The optimal circuit configuration uses a100 uA stimulation current, an active signal source, and a band pass filter at the output.

3.1.2 Revisions 2 and 3

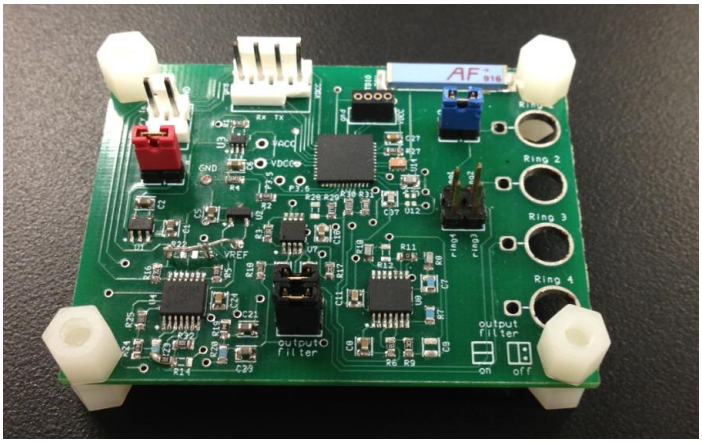

Figure 10. PCB Revision Two

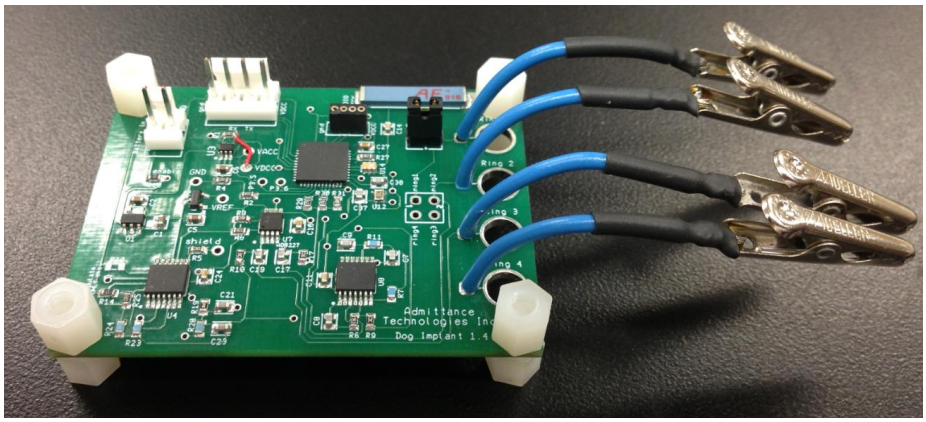

Figure 11. PCB Revision Three

Revisions two and three are only slightly different from one another. In revision two, wireless functionality started working with limited range. This revision also removed most of the circuit configuration options from revision one. Only the option to enable or disable the output band-pass filter was left. In revision three, this option was removed, leaving the output band-pass filter permanently enabled. Revision three modified the layout of the RF components. All RF passive components were moved as close to the processor as possible. Additionally, the signal trace to the antenna was significantly thickened to achieve 50 ohm single ended trace impedance, as required by the data sheet for the antenna and balun filter. Lastly, revision three modified the way that the circuit connects to calibration elements and pacing electrodes. Permanently attached alligator clips were manufactured and soldered to the device. This feature removed variability in connectors used with the circuit.

3.1.3 Revisions 4 and 5

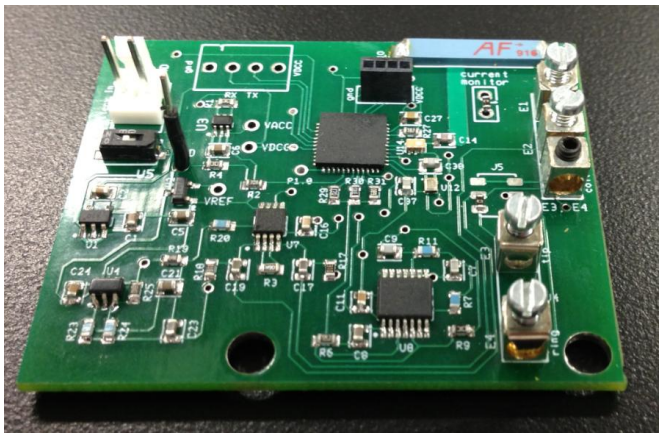

Figure 12. PCB Revision Four

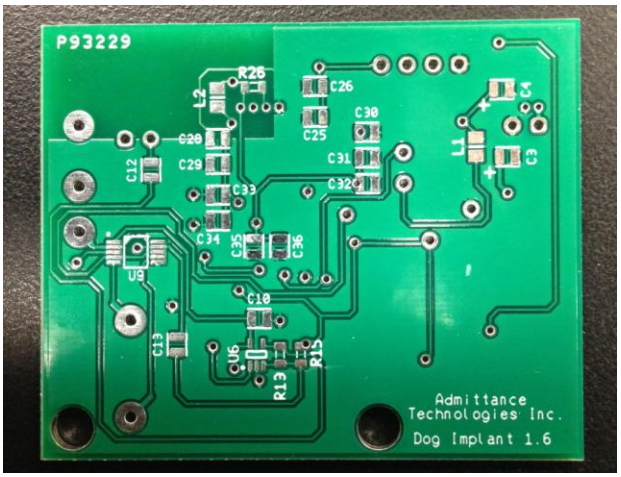

Figure 13. PCB Revision Five

Revisions four and five made minimal electrical changes and significant form factor changes. In revision four, the analog supply voltage was altered. Instead of being generated directly from the battery voltage it was decided that the analog supply should be generated from the regulated digital supply. By deriving the analog supply voltage from the digital supply, a stable system voltage is supplied to the device over the battery life-cycle. This is important because instrumentation phase offset drifts with supply voltage. The use of screw tap terminals instead of alligator clips was the biggest form factor change. This type of connection mimics the connectors found in a traditional pacemaker. This functionality is important for the device to become an implant. Additionally, a mechanical switch was added to allow quick switching between the two different measurement configurations. The physical size of the device was also optimized in this revision. In revision five, a layout issue with the wireless communication was corrected. Per the data sheet, the antenna is not supposed to have a ground plane underneath it. After fixing this issue, wireless range increased fivefold.

3.2 Attaching Processor (Wipe Soldering)

The processor is attached using a technique known as “wipe soldering”. The process starts by attaching the ground pad underneath the processor. A minimal amount of solder paste is

applied to the square pad in the center of the footprint using a syringe. The processor is then placed on the footprint, taking special care to align the processor pins with the pads of the footprint. Using a heat gun, the solder paste on the center pad is reflowed. The heat gun should be set 500 °F on the lowest airflow setting. 500 °F is the necessary reflow temperature, and the lowest airflow setting prevents the heat gun from blowing the processor off the footprint. Once firmly attached to the ground pad, the wipe soldering can begin. Using a flux pin, apply flux to each of the four processor edges. A micro-tip soldering iron set to 680 °F is then used to solder the processor pins. Create a small bead of liquid solder on the tip of the iron from a spool of thin and soft solder. Under a microscope, wipe the iron across one of the edges of the processor where it meets with the footprint. Care should be taken not apply to much pressure while wiping the iron across the edge of the processor, occasionally this can rip out the pads. Some of the processor pads will be fused together. To fix this, take the iron and run it between the bridged pads. Repeat this process for the other three edges of the processor.

3.3 Passive Component Matching and Tolerances

Specific components in the design must adhere to strict tolerances to ensure proper filter pass bands and high common mode rejection ratio (CMRR) in differential sections of the design. The low pass filter that handles signal conditioning for the current source must be constructed with ±1% resistors and ±5% capacitors. Similarly, the band pass filter at the output must be constructed with the same component tolerances. In general, the higher the quality factor (Q) of the filter the more important component tolerances are. Extreme care must be taken to match the components at the input to the instrumentation amplifier. A simple passive high pass filter is placed at the input to both the plus and minus terminals of the instrumentation amplifier. The purpose of the high pass filter is to re-reference the DC potential of the impedance signal to

system reference voltage. Therefore, its corner frequency should be placed far enough away from the signal frequency of interest so that gain and phase interactions do not occur. In this system, the corner frequency was placed at 15.9 Hz. It is very important that both the plus and minus input terminal have corner frequencies that are close to one another because this significantly effects the effective CMRR of the instrumentation amplifier. For this reason, ±1% capacitors and ±.1% resistors are used. Additionally, components within each batch of components are matched by hand to tighten the tolerances even further.

3.4 Important Active Component Specifications

To ensure the effective operation of the circuit, amplifier slew rate and voltage reference sink/source current should be properly selected. The impedance signal is measured with a 20 kHz sinusoid with maximum amplitude of 1 V. This yields an effective signal slew rate of ~.125 V/ µS. In this bio-impedance application phase information is extremely important. To ensure the stability of phase measurements, op-amps and instrumentation amps with 5X slew rate should be used. The instrumentation amplifier AD8227 has a slew rate of .8 V/ µS and the operational amplifier OPA376 has a slew rate of 2 V/ µS. Additionally, many voltage references are not designed to both sink and source current. In this application, the voltage reference must be able both sink and source current. The TI REF3125 selected is capable of ±10 mA.

Chapter 4: Device Calibration and Testing

4.1 Stimulation Current Magnitude Stability

The 100 uA RMS 20 kHz current source is a key component in the bioimpedance measurement system. Its stability is important for high precision impedance measurements. The current source must be able to activate and stabilize quickly in order for low-power operation to be possible. While active, its output current must not drift. Additionally, the source must be stable across a wide range of loads. This component of the device was extensively tested to ensure quality of measurement.

4.1.1 Warm-up and Drift Test

The current source was tested for warm-up time and drift using a fixed load of 50 ohms and a Fluke multi-meter capable of measuring true RMS current. The device was programmed with test firmware that continuously takes impedance measurements in a loop. The effect is a continuous stimulation waveform. Using the current breakout jumper, the Fluke was connected in series with the 50 ohm load and the RMS current was measured. With the help of a stop watch, the display current was recorded at routine intervals. The results show that the current source does not drift over the course of hours, and has a sub millisecond warm-up time.

Table 3: Current Source Warm-up and Drift

Time (minutes)	Current (uV RMS)
0	99.9
1	99.89
5	99.88
10	99.88
20	99.87
30	99.87
60	99.87
120	99.88

4.1.2 Resistor Sweep Test

The device is intended to work with a wide range of pacing electrodes, and each of these electrodes will have varying electrode-electrolyte interface properties. The current source must be able to drive stimulation current through all of these electrode-electrolyte interfaces. Simply put, it must be functional over a wide range of test loads. To test this, the same firmware and measurement setup from the warm-up and drift test were used. A variable resistor box was connected to the device. The load was swept from 1 ohm to 5000 ohms. The results show that the current source is relatively stable over a large load range.

Table 4: Current Source Resistor Sweep

Load (ohms)	Current (uA RMS)
1	99.89
10	99.85
50	99.69
100	99.5
200	99.39
300	99.39
500	99.37
1000	99.38
2000	99.45
5000	99.91

4.2 Output Waveform Stability

The analog bioimpedance signal must adhere to certain amplitude and frequency requirements. The output signal's amplitude when connected to the maximum of the load range is not to exceed 1V peak and should be centered at 1.25 V. This requirement ensures that the sinusoidal impedance signal will be bounded between .25V and 2.25V. The analog to digital conversion (ADC) reference on the CC430F5137 microcontroller is 2.5V. By adhering to these signal requirements no ADC clipping will occur. The bioimpedance signal is measured using a

20 kHz stimulation current. Given the stability of the current source, the final output waveform should also be 20 kHz. Ideally, the frequency of this signal will be tightly bounded over time, and have a low frequency jitter.

To test both frequency and amplitude stability of the output waveform, the device was placed in continuous test mode. In continuous test mode, a constant stimulation current is generated by running "admittance acquire" data in a loop. The device was connected to a 50 ohm load. An oscilloscope measurement was made at the input to the analog to digital converter. Amplitude and frequency measurements where then made by capturing a single oscilloscope fram. Amplitude measurements were performed using the horizontal cursors and period measurements were made using the vertical cursors. Ten sample functions of the output waveform were taken at random. The corresponding measurements are listed in the table below.

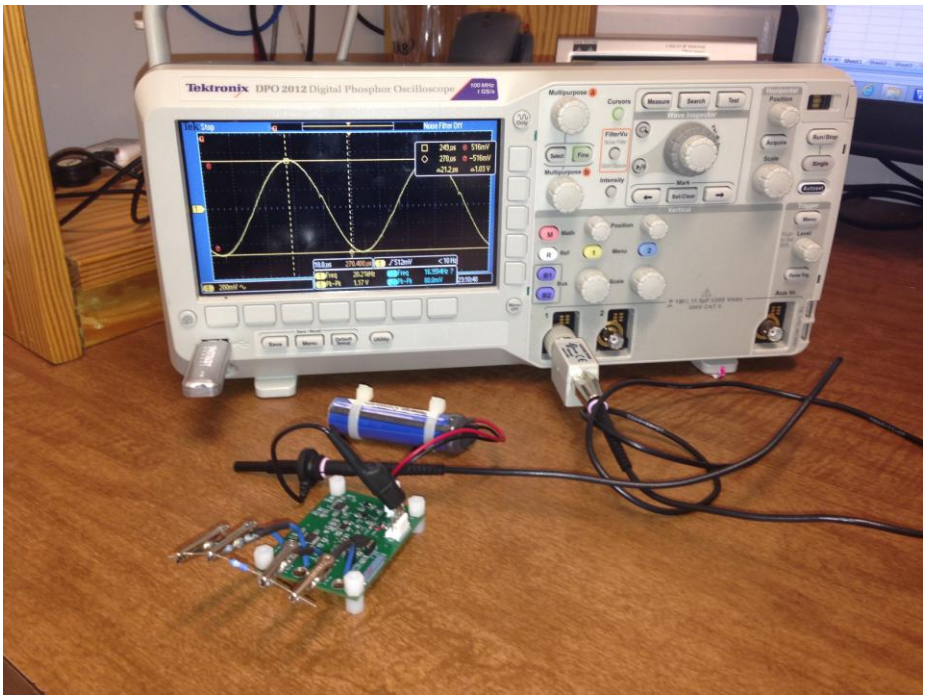

Figure 14. Amplitude Jitter and Test Setup

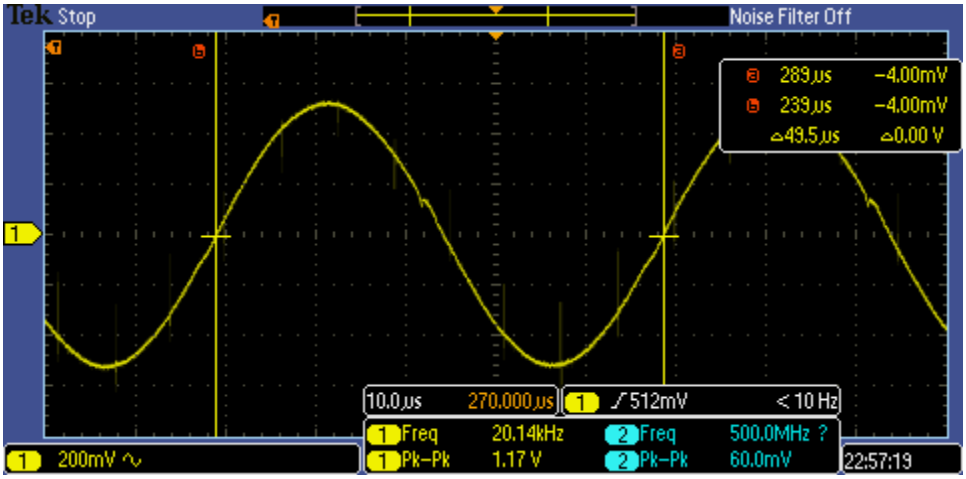

Figure 15. Frequency Jitter

Table 5: Output Waveform Stability Frequency and Amplitude

Test Number	Period (us)	Frequency (Hz)	Pk-Pk (V)
1	49.5	20202.0202	1.03
2	49.5	20202.0202	1.03
3	49.5	20202.0202	1.03
4	49.5	20202.0202	1.03
5	49.7	20120.72435	1.03
6	49.3	20283.97566	1.03
7	49.5	20202.0202	1.03
8	49.7	20120.72435	1.03
9	49.5	20202.0202	1.03
10	49.5	20202.0202	1.03
Average	49.52	20193.95658	1.03

The amplitude appears to be very stable, and although the frequency has some fluctuation the results can be explained. The oscilloscope that was used has a period resolution of .2 µs. Since the fluctuations seen were ± one resolution period the results can not accepted as truth. To better understand the frequency jitter of the system an oscilloscope with better period resolution must be used.

4.3 Sample and Hold Time Configuration

The CC430F5137 allows the user to configure the hold time of the built in analog to digital converter. For proper sampling, the hold time must adhere to specific timing requirements. The following equation can be found on page 425 of the CC430 user manual.

$$tsample > (Rs + 1.8\ k\Omega) \times \ln(2n + 1)\ \times 25pF + 800ns$$

Since the input to the ADC is driven by an op-amp RS can be set to zero. By substitution, "tsample" is equal to 973 ns. The ADC12CTL0 register allows the user to control the number of clock cycles the ADC will hold samples for. The register can be configured in powers of 2. In this system, the clock frequency of the ADC is configured to be 5 MHz. By division, this yields a hold time of 4.85 clock cycles. The closest power of 2 that satisfies this requirement is 8 clock cycles. For more information on register configuration refer to page 438 of the user manual [15].

4.4 Instrumentation Phase Offset and Calibration

Before use, the device must be calibrated for phase offset. These phase offsets occur because of several independent instrument characteristics. The instrument has parasitic inductances, and capacitances. The active components delay the signal in time resulting in a phase delay. There is a fixed time delay between DAC output and ADC sampling. These factors as well as others cumulatively add to instrumentation phase offset. Ideally, when measuring a purely resistive load the instrument should yield a zero phase measurement. For this reason, calibration is performed using resistors. It has empirically been shown that the instrumentation phase offset is variable with load. It has been proposed that the phase contributions of the active components are variable with signal amplitude. To solve this problem, the calibration is performed across a range of resistive loads that covers the entire measurement range.

This process begins by collecting a series of resistors that span the measurement range. At 20 kHz, the magnitude of intraventricular bioimpedances range from 20 to 40 ohms. Hence, a

set of 7 calibration resistors ranging from 10 to 91 ohms were used to calibrate the device. Using the “buckstopper.pde” processing script, 1000 samples are taken at each resistor value. The “Cicruit_Cal_Large_Animal_Final.m” matlab script is then used to generate calibration coefficients for the device. Additionally, the matlab script generates graphs for visual inspection of a quality calibration. An example calibration is provided bellow. The calibration outputs two graphs and one table. The outputs are shown bellow.

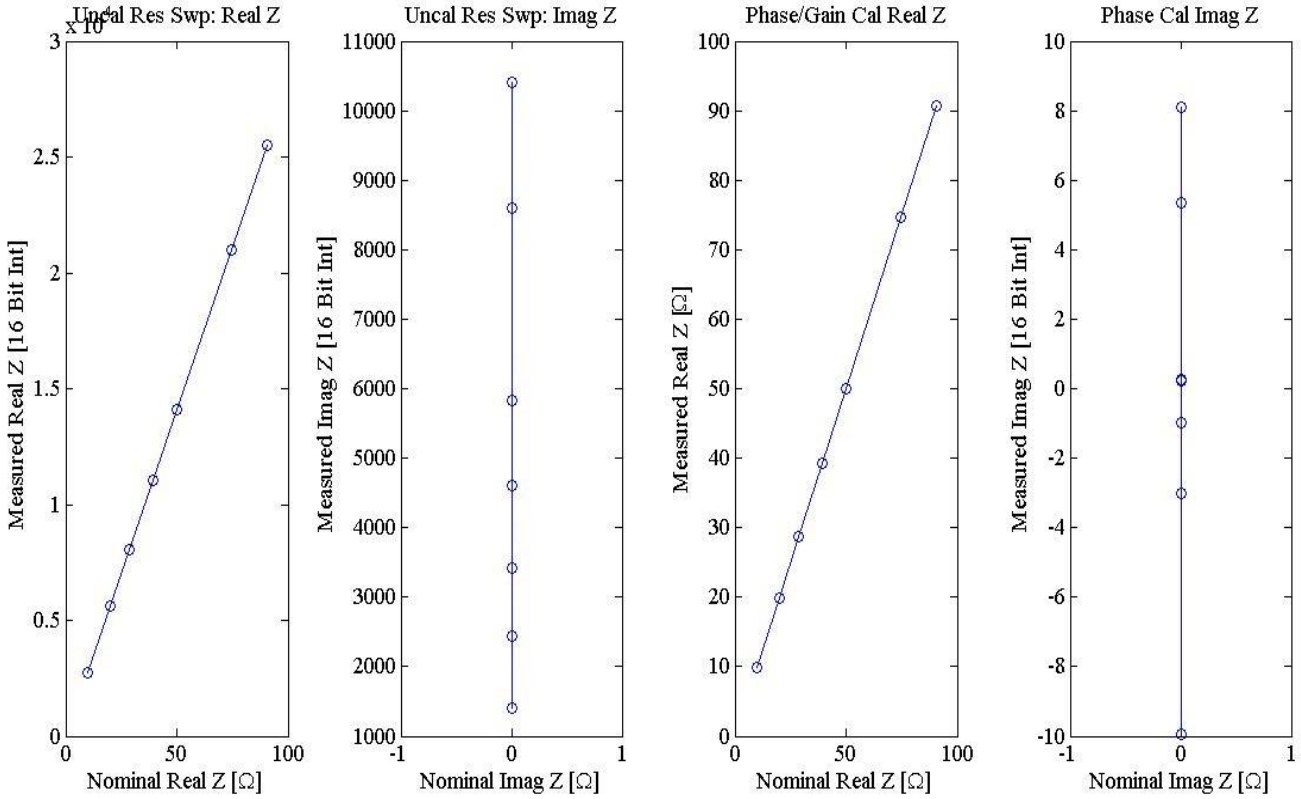

Figure 16(a,b,c,d left to right). Resistor Sweep Calibration Results

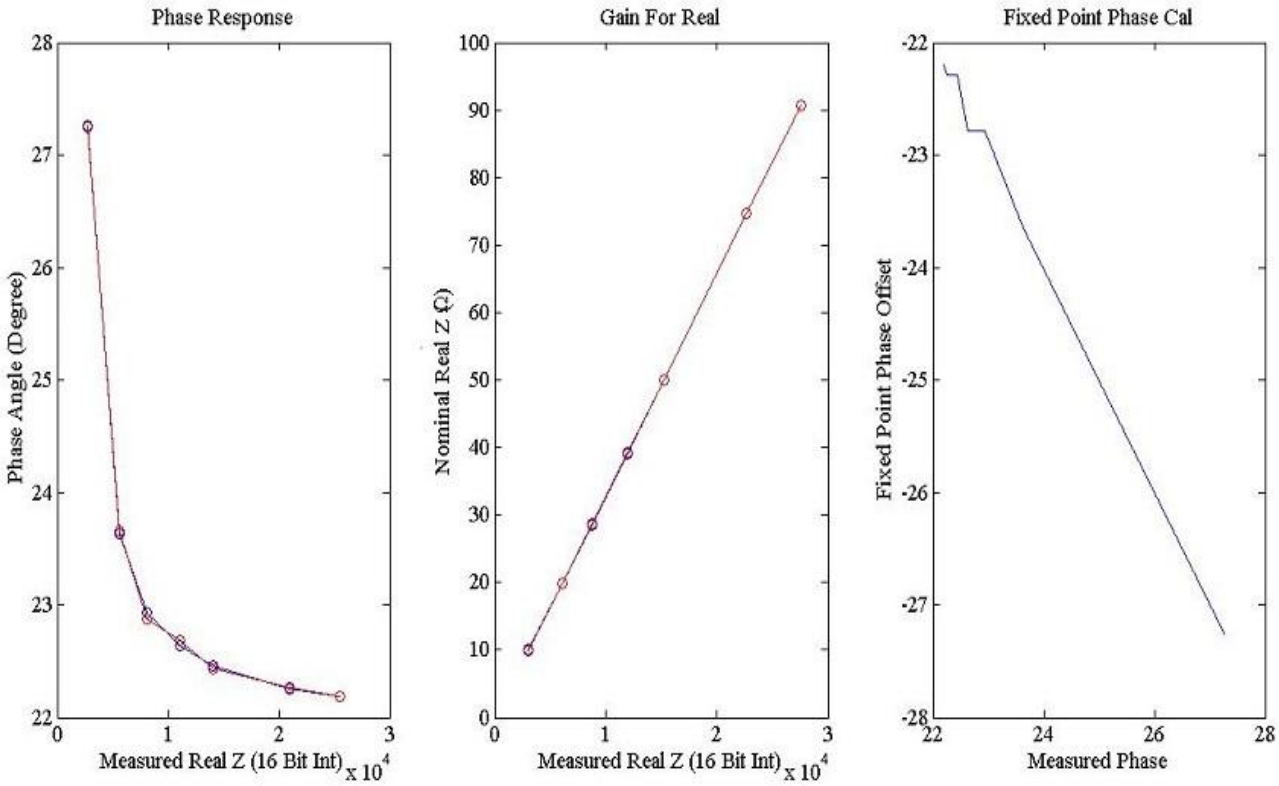

Figure 17(a,b,c left to right). Resistor Sweep Calibration Curves

Table 6: Embedded Calibration Arrays

```
int adc_val_c1[7]={2727,5596,8061,11038,14094,21000,25495,};
long real_calibration_c1[7]={625,500,50,50,100,100,125,};
long imag_calibration_c1[7]={-322,-219,-21,-21,-41,-41,-51,};
long divide_calibration_c1[7]={213068,165424,16435,16435,32754,32754,40913,};
long offset_calibration_c1=-25;
```

The calibration results from Fig 16 , Fig 17, and Table 6 display a quality calibration. In figure 15, the first two graphs represent the uncalibrated real and imaginary components of the impedance signal. In a resistor sweep, the measured real impedance and the nominal real impedance should be equivalent. In short, if you measure a 50 ohm resistor the device should yield a 50 ohm real impedance measurement. Additionally, the measured imaginary impedance and nominal impedance should always be zero. When measuring a resistor, there is not an imaginary impedance component. Clearly, the uncalibrated data is not representative of the expected result.

The first step in calibration is to compensate for instrumentation phase offset. To do this, fig. 17a is used. This graph shows a trend of measured phase angle as a function of the measured real impedance. In theory, the instrumentation phase offset should be a constant. However, in practice it is a function of the signal amplitude, and is termed “Load Dependent Phase Offset”. In this calibration, there is a load dependent phase range of approximately 5°. In a quality calibration this number can vary from 2° to 6° depending on process variations in the instrumentation and operational amplifiers used in the design. To reverse the phase offset, the phase is essentially zeroed while preserving the magnitude of the complex number. This can be accomplished by multiplying by a complex number with unit magnitude and a phase that is the inverse of the offset.

Now that the phase of the measured impedance has been corrected, the impedance measurement must be multiplied by a gain factor. The purpose of this is to relate the uncalibrated impedance measurement to the actual resistor value that is being measured. Fig. 17b shows that a linear relationship between the phase calibrated impedance measurement and the nominal impedance value exists. In reality, the equation for the line relating the two values has a very small offset. Hence, only a scalar value is necessary to relate nominal impedance to measured impedance.

After applying both phase and gain calibration to the uncalibrated impedance sample it can be seen that the resulting impedance sample approaches ideal. Fig. 16c shows a line of identity between nominal and measured real impedance values. Fig. 16d shows imaginary impedance values after phase calibration, but before gain calibration. It can be seen that the calibrated imaginary impedance has decreased by a factor of 1000 when compared to the uncalibrated imaginary impedance. Once multiplied by the scaling factor it is essentially zero. As

expected, when measuring a purely resistive load the system should yield the value of the resistor in the real and zero in the imaginary. Note that the imaginary measurements shown in the first graph are not multiplied by the scaling factor yet.

At this point, the calibration is moved to the embedded device. This is done to ensure that each device keeps track of its own calibration. This calibration could be performed after the impedance measurements have been wirelessly transmitted to the computer. However, with multiple devices there are multiple calibrations. By implementing the calibration on the embedded device the user need not worry about using different calibrations in the processing script that receives the wireless transmissions. The calibrations are implemented efficiently in fixed point. The matlab script automatically generates the fixed point calibrations. Since the calibrations are done in fixed point there is a precision limitation. The third graph in figure 16 displays the results of these auto generated calibrations. Ideally, this graph should be a inverse line of identity relating phase offset to phase calibration. Table 6 contains the calibration arrays used on the embedded device. These arrays are auto generated by the matlab script as well.

4.5 Complex Impedance Measurement Testing

The accuracy of complex impedance measurements produced by the device were analyzed extensively. To do this, a series of complex loads that cover the entire measurement range were used. For each load value, 1000 samples were taken using the device. For each set of 1000 samples standard deviation (STD) and expected value (EV) were calculated. Percent of measurement error is calculated by comparing the expected value of the samples to the calculated impedance of the load. Standard deviation is used to estimate noise in the measurement. A measure of signal to noise ratio (SNR) is calculated by dividing the expected value by the standard deviation.

$$SNR = \frac{EV}{STD}$$

Table 7: Expected Value and Standard Deviation

Res(Ω)	Cap (nF)	Calc ReZ (Ω)	Calc ImZ (Ω)	EV ReZ (Ω)	STD ReZ	EV ImZ (Ω)	STD ImZ
49.77	23.5	48.69691305	-7.228832679	48.71690647	0.011151125	-7.219842948	0.032141474
49.77	49.6	45.3210169	-14.19973374	45.35357401	0.020689677	-14.38585021	0.037001558
49.77	101	35.37204826	-22.56734463	35.67054801	0.019186612	-21.99051786	0.017797565
28.56	23.5	28.35425333	-2.415324676	28.37381209	0.008972371	-2.385258657	0.02482607
28.56	49.6	27.66569867	-4.974079929	27.6447867	0.008751082	-5.00356856	0.019103565
28.56	101	25.18438451	-9.220238523	25.11609021	0.011588914	-9.430758526	0.018341566
10.03	23.5	10.02103165	-0.299786773	10.0425261	0.004992959	-0.334473291	0.010467682
10.03	101	9.866887492	-1.26862633	9.86518718	0.00497143	-1.314669526	0.009106174

In the above table the test loads and their corresponding calculated and measured impedances are given. Intraventricular bioimpedance signals range from 20-j1 ohm to 40-j10 ohm. The test loads are representative of this range. In all cases, resistors and capacitors were placed in parallel with one another. Calculated impedances were made using a parallel circuit model, circuit values measured with a precision fluke multimeter, and a 20200 Hz frequency. The expected value (EV) and standard deviation (STD) of 1000 measurements taken by the device at each test load are also given.

Table 8: Percent of Measurement Error

Resistor (Ω)	Capacitor (nF)	% Measurement Error ReZ	% Measurement Error ImZ
49.77	23.5	0.041056843	0.124359367
49.77	49.6	0.071836664	1.310703927
49.77	101	0.843885955	2.556024104
28.56	23.5	0.068979987	1.244802382
28.56	49.6	0.075588084	0.592845927
28.56	101	0.271177181	2.283238146
10.03	23.5	0.214493381	11.57039639
10.03	101	0.017232512	3.629374182

The percent of measurement error for the device is given above. The results of the percent of measurement error for the real part of impedance show a high level of accuracy. The imaginary component of impedance is less accurate when compared to the real component. However, the largest inaccuracies occur with test loads that are not realistic for intraventricular bioimpedance measurements. In short, low magnitude measurements and measurements with phase angles greater than 30° are unrealistic. Even so, the percent of measurement error for the imaginary component is acceptable.

Table 9: Signal to Noise Ratio

Resistor (Ω)	Capacitor (nF)	SNR ReZ	SNR ImZ
49.77	23.5	4368.788588	224.6270047
49.77	49.6	2192.08707	388.7903946
49.77	101	1859.137421	1235.591388
28.56	23.5	3162.353718	96.07878451
28.56	49.6	3159.013442	261.9180479
28.56	101	2167.251493	514.1741215
10.03	23.5	2011.337656	31.95294688
10.03	101	1984.376156	144.3712293

The signal to noise ratio (SNR) of the device is provided in the above table. The SNR for the real component of impedance appears to scale inversely with capacitance. However, no apparent trend for the SNR of the imaginary component has been recognized. By analyzing the STD of the measured values it can be seen that the noise of the measured real and imaginary components of the signal is not a constant. The function that relates this noise to its corresponding load has not yet been identified. From the graph, one thing is clear; the device has a higher SNR for the real component within the measurement range of interest.

4.6 Maximum Sampling Rate

The device software runs open-loop in order to take impedance measurements as fast as possible. The software sequentially takes raw data samples, calculates an impedance sample,

calibrates the sample, and finally wirelessly transmits the sample. A timer interrupt is not used to enforce a fixed frequency of this sequential action, code runs in an open loop as fast as possible. In order to properly analyze the data, it is important to know the exact frequency that the device takes impedance measurements at. To do this, an oscilloscope was used to measure the time period between current stimulation pulses. An example oscilloscope measurement is provided bellow.

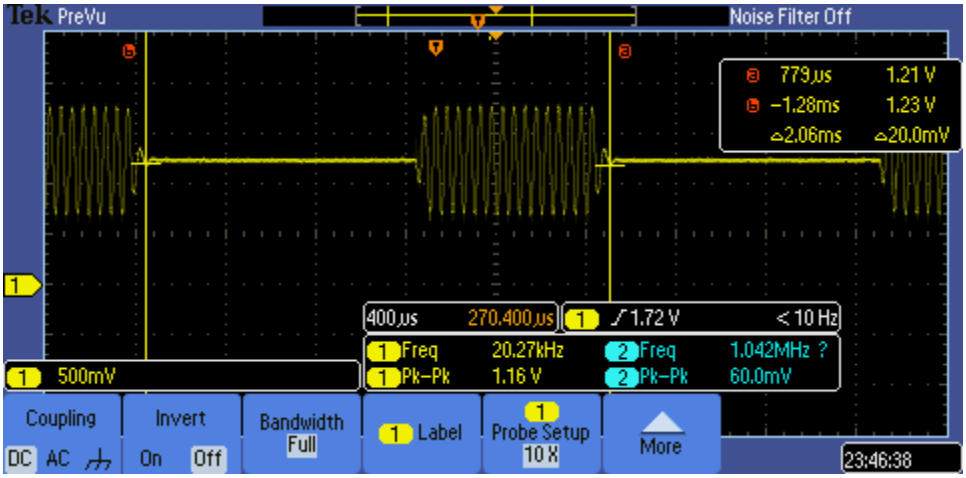

Figure 18. Maximum Sampling Period Measurement

The time period between pulses was measured using the horizontal cursor measurement feature. As shown, the calculated period is 2.06 ms. Hence, the sampling rate is 485 Hz. This sampling rate is significantly higher than the maximum heart frequency of interest. Assuming a maximum heart rate of 220 beats per minute (BPM) and useful information up to the 3rd harmonic the maximum frequency is 11 Hz. Since the heart signal is greatly oversampled by the device it is possible to do accurate time-based analysis.

Chapter 5: Electrode Configurations, Calibration, and Saline Experiments

5.1 Tri-polar Configuration

The tri-polar electrode configuration can used to measure impedance data related to volume in the right ventricle (RV) of the heart. Standard right ventricular shocking leads come equipped with 3 independent electrical contacts. Ideally, impedance measurements should be made using four contacts. In this way, stimulation pathways and sensing pathways can be separated from each other. This method minimizes the effects of the electrode electrolyte interface that reduce accuracy in the impedance measurement. The tri-polar measurement is not ideal; however, given the available RV shocking lead it is the best possible measurement configuration.

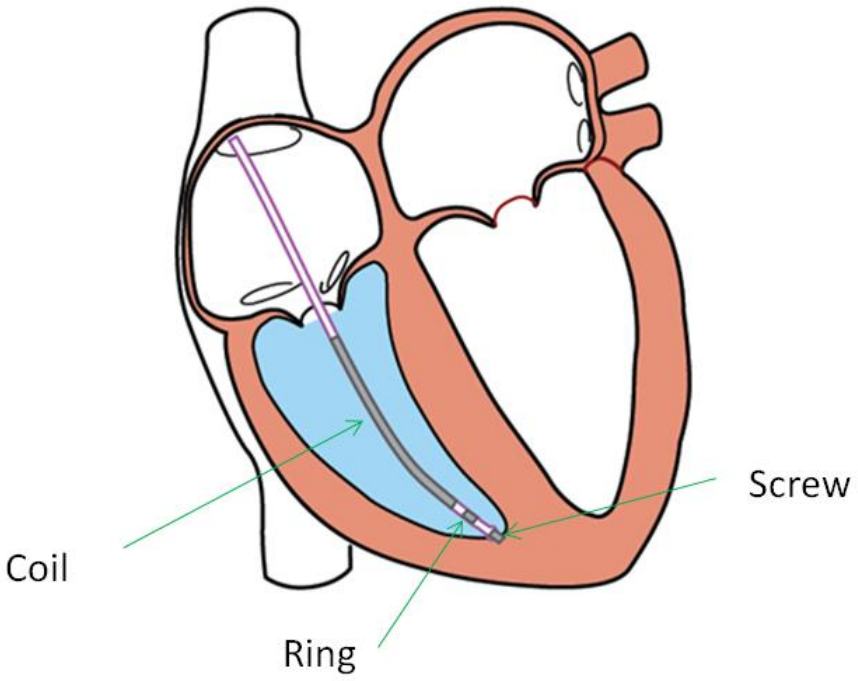

Figure 19. Tri-polar Electrode Configuration

In the above image three electrical contacts comprise the RV shocking lead. From top to bottom these contacts are: coil, ring, and screw. One of these contacts must act as both a stimulation node and a sensing node. The other two can act independently as either a sensing node or a stimulation node. The largest contact, the coil, is the ideal contact to act as a shared node. In practice, the configuration is as follows: coil is shared node, ring is sensing node, and screw is stimulation node.

5.1.1 Analysis Techniques

To analyze RV tri-polar data, a parallel circuit model of the blood and muscle is used. For reference, parallel circuit models were discussed in chapter 1. An equation for removing the muscular component of the impedance signal has been developed in previous research in our group [5]. The equation is formulated in terms of the measured Admittance Y. Additionally; the equation is formulated using the empirically measured tissue properties (σ/ϵ) ratio in order to remove the impedance contribution from the muscle. This ratio defines a fixed relationship between the resistive and capacitive properties in myocardial tissue. The following equation isolates G_b, the conductance of blood.

$$G_b = Re\{Y\} - G_m = Re\{Y\} - \frac{[Im\{Y\} - \omega C_{probe}]}{\omega}\frac{\sigma_m}{\epsilon_m}$$

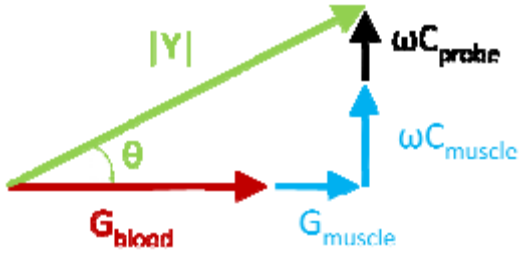

Figure 20. Admittance Method

5.1.2 Volume Sensitivity

Saline experiments have been conducted to prove that the tri-polar electrode configuration is sensitive to changes in volume. In the experiment, impedance measurements were taken in different sized cuvettes. Overall cuvette volumes ranged from 7.9 ml to 50.3 ml. Cuvettes were filled with 8300 (uS/cm) conductivity solution. Impedance measurements were taken in each of the cuvettes recorded, and plotted in terms of admittance Y.

Table 10. Tri-polar Volume Results

Cuvette #	R (mm)	Volume (mL)	Mag |Y| (µS)	Phase Y (°)
1	15.9	7.9	32642	-2.38
2	17.5	9.6	40147	-2.15
3	19.1	11.5	44088	-2.01
4	29.5	27.3	59707	-1.58
5	34	36.3	62381	-1.74
6	40	50.3	61918	-1.76

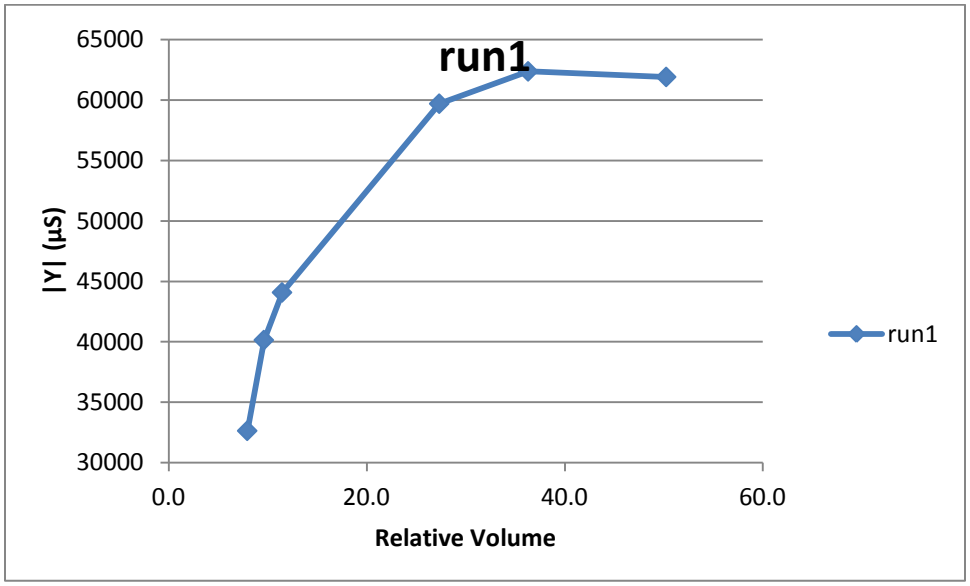

Figure 21. Tri-polar volume graph

Fig. 21 shows that the bulk admittance measured by the system increases as the volume of solution is increases. It can also be seen that the measured admittance trends towards a maximum value as the volume increases. This is because the associated current density decays

rapidly moving away from the origin of stimulation. Hence, the associated current density very far away from the origin of stimulation is negligible.

5.2 Tetra-polar Configuration

. The tetra-polar configuration usually used to make left-ventricular impedance measurements. In this configuration, the electrical contacts are split between two independent pacing leads. Two of the contacts are associated with the ring and screw of the RV shocking lead. The other two contacts are associated with the ring and the tip of the bi-ventricular lead that is snaked through the coronary sinus and rests in posterior vein of the left ventricle. In this way, one stimulation node and one sensing node are associated with each of the independent pacing leads. In an ideal impedance measurement, the distance between electrodes should be fixed. Therefore, it is ideal to have all nodes on a single lead. However, it is physiologically unacceptable to permanently implant a lead inside the left ventricle. Therefore, a cross-ventricular impedance measurement is made using two independent leads.

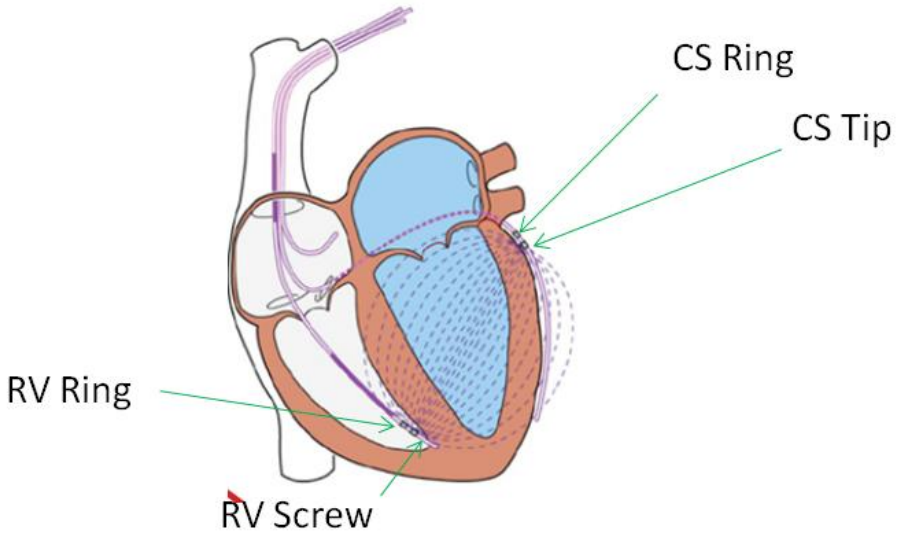

Figure 22. Tetra-polar Configuration

In fig. 21 it can be seen that the measurement is made across the left-ventricle of the heart using two independent pacing leads. The field geometry sketch is provided purely for the purpose of illustration, and does not represent the actual electro-magnetic field of the system.

5.2.1 Analysis Techniques

Similarly to the tri-polar configuration, the same technique is used to remove unwanted impedance contributions from the muscle. The formulation of this model was originally proposed by Porterfield [3], and has since been revised by Larson [2]. The model rests on the assumptions of an idealized first order approximation of the equivalent circuit model for the system. Refer to the series parallel model that was discussed in chapter 1. The equation is formulated in terms of impedance Z, and also takes advantage of the (σ/ϵ) ratio described in the previous section.

$$R_b = Re\{Z\} + \frac{Im\{Z\}}{\omega}\frac{\sigma}{\epsilon}$$

5.2.2 Distance Sensitivity

Saline experiments have been conducted to show that tetra-polar impedance measurements in a cross ventricular configuration are correlated with distance. In the experiment, a large plastic vessel of 7000 (uS/cm) saline was used. A stationary RV shocking lead was placed in the saline 2 inches away from the wall of the plastic vessel. A second bi-ventricular pacing lead was placed in the saline at a varying distance away from the RV shocking lead. The distance between the two leads was varied from 5 to 80 mm. Impedance measurements were taken and plotted as a function of distance.

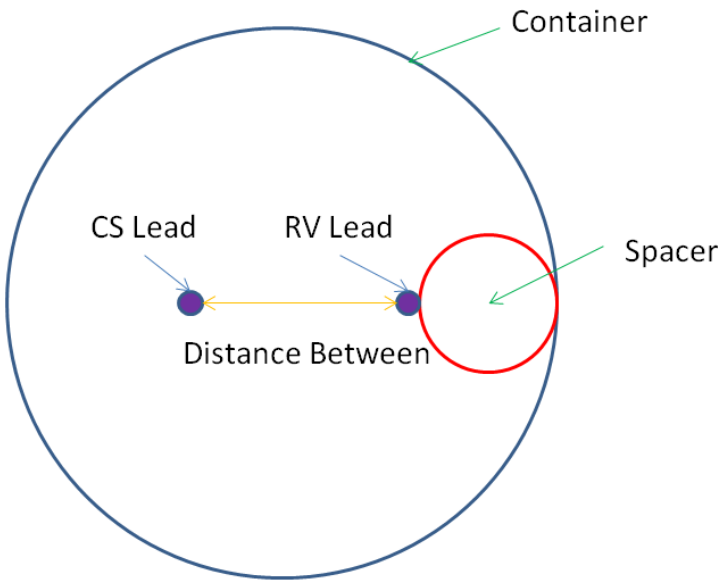

Figure 23. Distance Experiment Setup

Table 11. Cross Ventricular Tetra-polar Experiment

Distance mm	Real (ohms)	Imaginary (ohms)
5	1.56	0.8
10	5.61	0.76
15	8.78	0.4
20	10.96	0.28
25	12.5	0.23
30	13.61	0.22
35	14.74	0.21
40	15.64	0.03
45	16.5	0.01
50	17.19	0
55	17.94	0
60	18.58	-0.01
65	19.33	-0.01
70	20.03	-0.02
75	20.84	-0.02
80	21.72	-0.03

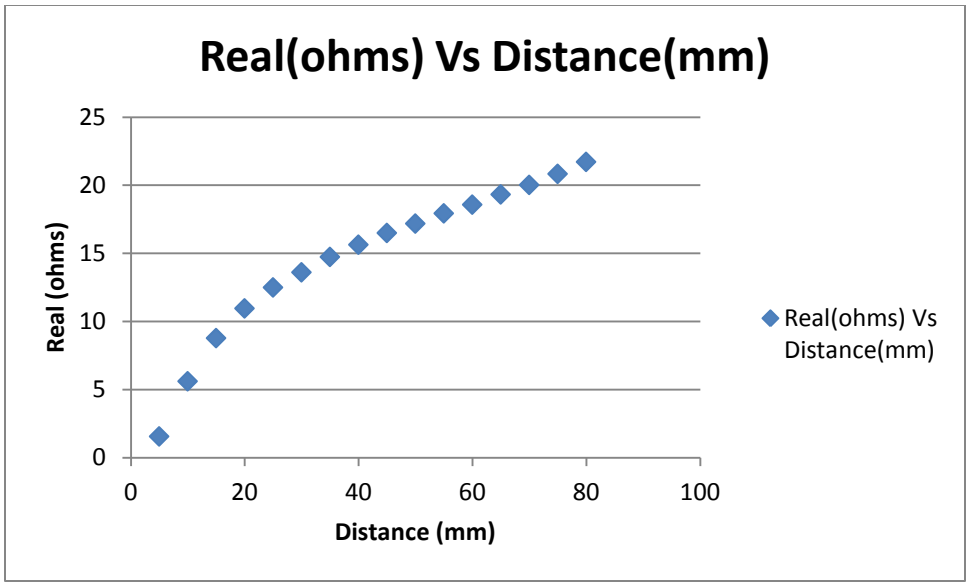

Figure 24. Cross Ventricular Tetra-polar Experiment Real

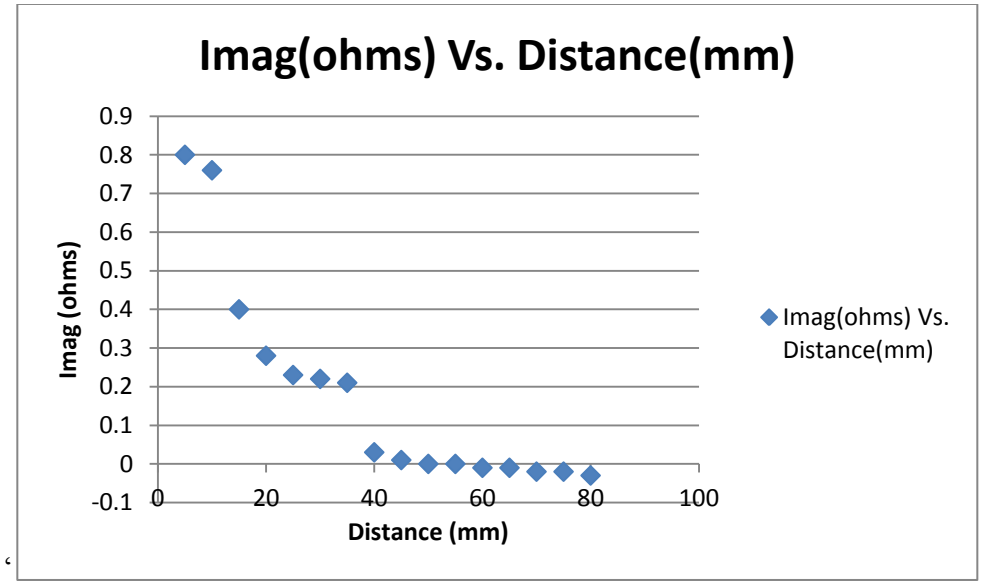

Figure 25. Cross Ventricular Tetra-polar Experiment Imaginary

As the distance between electrodes increases the measured impedance increases. At the lower distances, non-idealities in the measurement system are more prevalent. From fig. 25, it can be seen that an imaginary impedance measurement of nearly one ohm is seen at the smallest distances. In saline, there should be a negligible imaginary contribution to the impedance signal.

It is possible that this is a calibration issue, or due to mutual capacitance between electrodes. In practice, impedance measurements across the left-ventricle of the heart are typically greater than 20 ohms, approximately 40 mm. In saline we expect the imaginary part of the impedance measurement to be zero. The measured imaginary impedance for distances greater than 40 mm approaches zero.

Chapter 6: Conclusion

6.1 Unresolved Problems

Unresolved problems still remain in both the circuit and the current data analysis methods.

From the data that has been collected to evaluate measurement error in the device, it is clear that the imaginary components of the impedance samples are less accurate than the real components. This is likely the result of load dependent phase issues that significantly affect the imaginary impedance component for the test loads of interest. As stated previously, this has largely been determined to be a slew rate limitation of the instrumentation amplifier. However, given the voltage and power limitations of the system, this instrumentation amplifier is best in class. Alternative solutions to this problem that still allow for a low power implementation would be a tremendous benefit to the accuracy of the device.

The current cross-ventricular tetra-polar analysis techniques are based largely on speculation and suffer from the limitations associated with a highly-idealized first order approximation of the problem. Additional studies in conscience ambulatory subjects are required, for both the right ventricular and cross-left ventricular measurement techniques, to study the effects of long term drift, motion, and respiration.

6.2 Future Direction

With the high accuracy low power bioimpedance measurement system fully developed, intraventricular monitoring of stroke volume in-vivo can begin. Additionally, an application of the device for the purpose of non-invasive external stroke volume measurements will be explored. Signal processing techniques to evaluate the data in real-time will also need to be developed for both potential applications.

In-vivo experimentation will focus on measuring right ventricular and cross-left ventricular impedance in cardiovascular physiologies similar to that of a human. In these experiments, cardiovascular physicians will implant pacing leads in orientations that mimic current human medical practices. Impedance measurements will then be taken while modulating stroke volume using known physiological mechanisms. For example, stroke volume can be modulated by: performing an inferior vena cava (IVC) occlusion, using a pacemaker to control heart rate [12], administering beta-adrenergic agonists or their opposing beta-adrenergic blockers [11], or through a controlled exercise routine. Trends in impedance measurements will then be evaluated and then correlated with stroke volume. In practice, a measure of "truth" for stroke volume does not exist. However, several approximate modalities are available. These include but are not limited to: thermal dilution with Swan Ganz catheter, aortic-cuff type flow probes, catheter type flow probes, 3D/2D trans-esophageal echo [13], and 3D/2D trans-thoracic echo. Before moving into *in-vivo* experiments these modalities must be thoroughly evaluated for their surgical complexity and relative accuracy.

In the 1960's impedance science behind impedance cardiography was developed. Overall, experimental results were found to be inaccurate and of little clinical significance [14]. However, cardiologists have expressed interest in a portable device that can be used to continually monitor the stroke volume of patients placed in intensive care as a result of severe cardiovascular events. The developed impedance device is wireless, low-power, and cost-effective making it an ideal candidate for portable continuous monitoring. For this to be possible, algorithms capable of removing respiration and motion artifact in real time must be developed.

Moving forward, research and development efforts will focus on creating signal processing algorithms to interpret bioimpedance signal reliably. These algorithms will focus

heavily on isolating relevant information about the cardiovascular system in the presence of multiple noise sources. These algorithms are expected to execute in real-time in a completely automated manor. Eventually, this technology has the potential to improve patient outcomes on a global scale.

If you don’t do it this year, you’ll be another year older when you do.

-Warren Miller

Appendix

Discrete Fourier Transform, DFT

Input: N time samples

$\{a_n\} = \{a_0, a_1, a_2, \ldots, a_{N-1}\}$

Output: a set of N frequency bins

$\{A_k\} = \{A_0, A_1, A_2, \ldots, A_{N-1}\}$

$$A_k = \sum_{n=0}^{N-1} a_n W_N^{kn} \qquad \text{where } W_N = e^{-j2\pi/N}$$

$k = 0,1,2,\ldots,N-1$

While the DFT deals only with samples and bins, with no concept of seconds and Hz, when looking at ADC samples spaced at intervals T (in sec). The equivalent sampling rate fs (Hz) is defined as 1/T (sec). Frequency bin k represents signal components around $k*f_S/N$ (in Hz). The value at each bin corresponds to the amount energy that the time sampled signal contains in the specific frequency range that the bin covers. The DFT resolution in Hz/bin is the reciprocal of the total time spent gathering time samples; i.e., 1/(NT).

The DFT is a powerful tool that can be used for a number of signal processing applications. These include but are not limited to the following: filtering, demodulation, and frequency profiling.

In the impedance device that was developed, the DFT was used for the purpose of demodulating the raw voltage samples measured by the system. A continues block of raw voltage samples were taken, and the DFT was used to measure the amount of energy at a specific frequency. Several methods for demodulation of a signal exist. However, the DFT was selected because it can be efficiently implemented in software, and has no hardware overhead.

References

[1] Loeffler, K. (2012). *Development of an implantable system to measure the pressure-volume relationship in ambulatory rodent hearts*. (Master's thesis).

[2] Larson, E. (2012). *Admittance measurement for assessment of cardiac hemodynamics in clinical and research applications*. (Dotoral Dissertation).

[3] Porterfield, J. (2010). *Admittance measurement for early detection of congestive heart failure*. (Doctoral dissertation).

[4] A. T. Kottam, J. Porterfield, K. Raghavan, D. Fernandez, M. D. Feldman, J. W. Valvano and J. A. Pearce, "Real time pressure-volume loops in mice using complex admittance: measurement and implications," *Proceedings of the 28th IEEE EMBS Annual International Conference*, pp. 4336-4339, 2006.

[5] J. E. Porterfield, A. T. Kottam, K. Raghavan, D. Escobedo, J. T. Jenkins, E. R. Larson, R. J. Trevino, J. W. Valvano, J. A. Pearce and M. D. Feldman, "Dynamic correction for parallel conductance, Gp, and gain factor, alpha, in invasive murine left ventricular volume measurements," *J. Appl. Physiol.*, vol. 107, pp. 1693-1703, 2009.

[6] Riatt, M. (2013). Inappropriate implantable defibrillator shocks an adverse outcome that can be prevented. *Journal of America College of Cardiology*,*62*(15), 1351-1352. Retrieved from http://content.onlinejacc.org/article.aspx?articleid=1699351

[7] P. B. Adamson, A. Magalski, F. Braunschweig, M. Bohm, D. Reynolds, D. Steinhaus, A. Luby, C. Linde, L. Ryden, B. Cremers, T. Takle, and T. Bennett, "Ongoing right ventricular hemodynamics in heart failure: clinical value of measurements derived from an implantable monitoring system," *J Am Coll Cardiol*, vol. 41, pp. 565-71, Feb 19 2003.

[8] Greenspon, A. (2012). Trends in permanent pacemaker implantation in the united states from 1993 to 2009: increasing complexity of patients and procedures.*Journal of America College of Cardiology*,*16*(60), 1540-1545. Retrieved from http://www.ncbi.nlm.nih.gov/pubmed/22999727

[9] *Implantable cardioverter-defibrillator (icd) - topic overview*. (2010, August 9). Retrieved from http://www.webmd.com/heart-disease/tc/implantable-cardioverter-defibrillator-icd-topic-overview

[10] Raghavan, K. (2009). Electrical conductivity and permittivity of murine myocardium. *IEEE Transaction on Biomedical Engineering*, *56*(8), doi: 0018-9294

[11] Merta, M., et al. "Beta-blocker therapy influences the hemodynamic response to inotropic agents in patients with heart failure." *J Am Coll Cardiol* 40 (2002): 1248-1258.

[12] Barber, Gerald, et al. "Hemodynamic responses to isolated increments in heart rate by atrial pacing after a Fontan procedure." *American heart journal* 115.4 (1988): 837-841.

[13] Nagueh, Sherif F., et al. "Recommendations for the evaluation of left ventricular diastolic function by echocardiography." *European Journal of Echocardiography*10.2 (2009): 165-193.

[14] Allen, Michael T., et al. "Methodological guidelines for impedance cardiography." *Psychophysiology* 27.1 (1990): 1-23.

[15] Texas Instruments. CC430 User's Guide. Dallas: 2010. Web. <http://www.ti.com/lit/ug/slau259e/slau259e.pdf>.